applied sciences

MDPI

Article

Preliminary Investigation of the Performance of an Engine Equipped with an Advanced Axial Turbocharger Turbine

Gregory Guarda[1], Apostolos Pesyridis[1,2]* and Ashish Alex Sam[1]

[1] Department of Mechanical and Aerospace Engineering, Brunel University London, UB8 3PH, UK
Gregory.Guarda@brunel.ac.uk (G.G.), ashishalex.sam@vit.ac.in (A.S.)
[2] Alasala Colleges, King Fahad Bin Abdulaziz Rd., 31483, Dammam, Saudi Arabia

*Correspondence: a.pesyridis@brunel.ac.uk (A.P); Tel.: +44-1895-267901

Received: Accepted: Published: date

Abstract: Stringent emission regulations and increased demand for improved fuel economy has called for advanced turbo technologies in automotive engines. The use of turbochargers on smaller engines is one such concept but they are limited by the time delay to reach the required boost during transient operation. The amount of turbocharger lag plays a key role in the driver's perceived quality of a passenger vehicle's engines response. This paper investigates an alternative method to the conventional design of a turbocharger turbine to improve the transient response of a passenger vehicle. The investigation utilises the Ford Eco-Boost 1.6 litre petrol engine, an established production engine, equipped with a turbocharger of similar performance to the GT1548 produced by Honeywell. Commercially available Ricardo WAVE was used to model the engine. Comparing the steady state performance showed that the axial turbine provides higher efficiencies at all operating conditions of engine. The transient case demonstrated an improved transient response at all operating conditions of the engine. The study concluded that by designing a similar sized axial turbine, the mass moment of inertia can be reduced by 12.64% and transient response can be improved on average by 11.76%, with a maximum of 21.05% improvement. This study provides encouragement for the wider application of this turbine type to vehicles operating on dynamic driving cycles such as passenger vehicles, light commercial vehicles and certain off-road applications.

Keywords: turbocharger; axial turbine; genetic algorithms; multidisciplinary design optimisation

1. Introduction

During recent years, emissions legislation for automotive manufacturing has become more restrictive, requiring much more advanced exhaust after treatment systems. This requirement puts heavy demand on manufacturers to provide unique solutions to meet these targets. The downsizing of engines provides an alternative solution to reduce the emission levels produced in passenger cars, as well as improving fuel consumption. Spark ignition engines can have an expected 40% smaller displacement, along with 25% improved combustion performance by implementing a turbocharger [1]. The use of smaller engines, operating with less fuel than that of their larger counterparts directly reduces the amount of emissions produced, which in addition also reduces fuel consumption.

With the increase in turbocharged passenger vehicles, driver demand for reduced 'turbo lag' will likely follow, or from the driver's point of view, the delay in throttle response. Turbo lag is a measure of the time delay for a turbo spinning at a low speed, where no boost is produced, to be

brought up to the speed where it can function effectively [2]. The reduction of turbo lag can be associated with the design of the turbine component of the turbocharger, used to recover energy in the exhaust gases to mechanical energy. Turbo lag is mostly apparent at low engine speeds, where the exhaust mass flow rate is not sufficient to provide enough energy to drive the turbine. Many methods have been suggested and tested to reduce turbo lag, but fundamentally, the most important is reducing the mass moment of inertia. An alternative method suggested by the Ford Motor Company was the implementation of an axial inflow turbine to improve transient response [3].

Conventionally, turbocharger turbines employed in the automotive industry are radial inflow, whereby the exhaust gas enters the rotor radially and leaves axially. The axial turbine is different, in that the exhaust gases are axially guided by stationary guide vanes (stators) onto the rotor. Thus the flow through the rotor is predominantly in axial and tangential directions and there is no radial change in the flow across the rotor. The benefit of this method over its conventional counterpart is that it typically, at the same diameter, provides a higher total-to-static efficiency, and thus produces more power for the same flow conditions. This means that the axial rotor diameter can be reduced to produce the same power as its radial counter-part, thus reducing its mass and its inertia [4].

Even with lower inertia, like its radial counterpart, the axial turbine is still limited by turbo-lag, which is more evident at lower engine speeds and load conditions. Variable geometry turbines (VGT) technology is used to improve the performance of turbine at lower flow rates as well as higher flow rates, by interacting with the flow to change the velocity and flow angles to achieve better turbine performance. Literature also reports the use of mixed flow turbines in turbocharger applications [5, 6]. The use of mixed flow turbines reduces the inertia and they also provide a flat efficiency characteristic, enhancing the performance at lower blade speed ratios.

This paper however carries forward the analysis of an axial turbine concept carried out by Pesyridis et al [7, 8]. The objective of this paper is to analyse the transient response of the turbocharger system using the axial turbine and to compare it with a conventional radial turbine. By necessity certain assumptions are embedded (see section 3) and a detailed scaling method is presented (in section 2.2) in converting the turbine for appropriate use for this particular engine application. The methodologies and results presented below, are extensive using real-world engine data but did not intend to be applicable to the specific production engine. The methodology was based around the idea of proximity to the performance of a popular, mass production engine with the ultimate goal being the detailed comparison and discussion of the merits of the presented axial turbine versus the baseline radial turbine in current use.

2. Literature review

2.1 Axial Turbines for Turbocharging

Honeywell Turbo Technologies (HTT) presented a report detailing a breakthrough in the development of an axial turbine for improved transient response with their DualBoostTM turbocharger. The results demonstrated a reduction in turbo lag of 25%, by reducing the mass moment of inertia by 50% [9]. Figure 1 shows the comparison of the total to static efficiency between the newly developed DualBoostTM turbine and the baseline radial. The figure demonstrates that the axial turbine is more effective under the low velocity (blade tip to absolute gas flow velocity) ratios, in recovering the energy from the exhaust gas. However, the theoretical maximum efficiency of the axial turbine is lower than that of the radial turbine.

This technology, however, is not relatively new. Ford Motor Company conducted a testing in 1985 to assess the performance of an axial turbine when compared to a radial turbine on a 2.3-litre engine under transient conditions. The study identified that the axial turbine could produce the same “flow and peak efficiency characteristics” as its radial counterpart at different engine speeds but with a lower inertia. The results of the study demonstrated a 25% to 40% improvement on the transient response of the turbocharger with just under 50% mass moment of inertia reduction. This provides a target for the design considered in the present work to achieve at least a 25% improvement in transient response [3].

Despite the discussed advantages in the implementation of the axial turbines, there are few challenges associated with it. Axial turbines are predominantly found in aerospace and large power generation applications. For automotive turbochargers, as the power range is in kilowatts, blade height for axial turbines is comparatively smaller than radial turbines and would result in disproportionate increase in leakage flow effects. Therefore, a key challenge is the corresponding decrease in efficiency with a decrease in size. This calls for finer manufacturing tolerances and in turn makes the employment of axial turbines for turbocharger applications more costly [10]. Hence, increases in aerodynamic efficiency are of paramount importance in the successful employment of such designs. In addition, for the successful implementation of an axial turbine design, a detailed flow field and rotor dynamic analysis of the turbine needs to be performed followed by transient performance testing of the turbocharger and engine. This type of research is on-going but outside the scope of this paper.

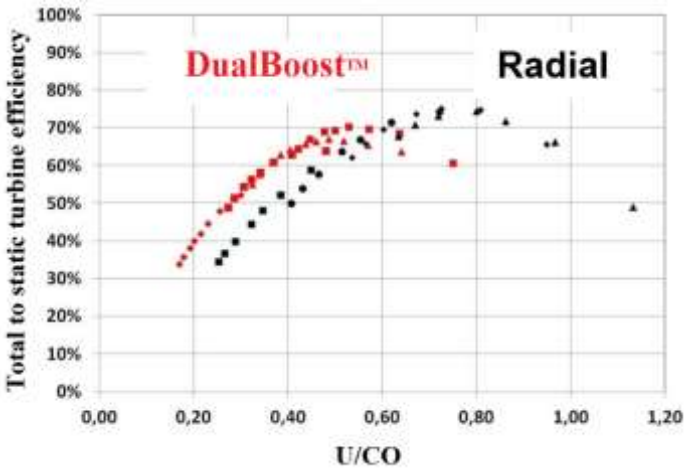

Figure 1. Comparison of turbine total to static efficiency vs blade to gas speed ratio between a radial and axial turbine [9].

2.2 Turbocharging map scaling

Matching a turbocharger map to any given engine model is a difficult task to accomplish; several different methods throughout literature have been attempted. However, all methods start with the same fundamental principle, of scaling the map in terms of dimensionless coefficients. By using this method, a map is obtained that is representative of a family of turbochargers of similar performances, but of different operating conditions and sizes. For turbomachinery in the gas turbine industry, the following scaling law relationship (Eq. 1) is used to define the pressure ratio as a function of rotor tip Mach number, the mass flow coefficient, the Reynolds number and the Mach number based on inlet conditions [11].

$$\frac{P_d}{P_u} = f\left[\frac{N_{TC}\ \ D}{\sqrt{RT_u}}, \frac{\dot{m}\sqrt{RT_u}}{P_u D^2}, R_e, M_n\right] \quad (1)$$

Equation 1 shows the pressure ratio for a compression process. For a turbine, it would be for the expansion process which would be the inverse of the left-hand side of Eq. 1, but the right hand side stays the same. The above equation allows for the ability to treat a tested turbocharger performance as a black box system, and similar pressure ratios can be obtained for compressors and turbines of the same family by keeping these parameters constant at each point. Thus, this assumption leads to the first stage used in most literature to scale maps to their dimensionless coefficients, giving a generic map that will govern the family. This is extremely useful when designing new equipment, as it is far easier and quicker to simply scale a map theoretically to test turbomachinery, at various diameters, then manufacture and test.

The laws can yield comparable results for differently sized turbomachinery; however an exact match between the similar turbomachinery cannot be achieved [12]. Therefore to simplify the scaling of turbomachinery it can be assumed for small scaling factors of diameter, the Reynolds number can be free to vary and the gas specific properties of the flow are constant [13]. This assumption has also been used in an alternative method for scaling using the polytropic infinitesimal stage [14]. Therefore when scaling, Eq. 1 can be further reduced to Eq. 2.

$$\frac{P_d}{P_u} = f\left[\frac{N_{TC}\ \ D}{\sqrt{T_u}}, \frac{\dot{m}\sqrt{T_u}}{P_u D^2}\right] \quad (2)$$

Equation 2 along with the black box treatment of the turbomachinery, can be better put into context by looking at a performance map shown below in Fig. 2.

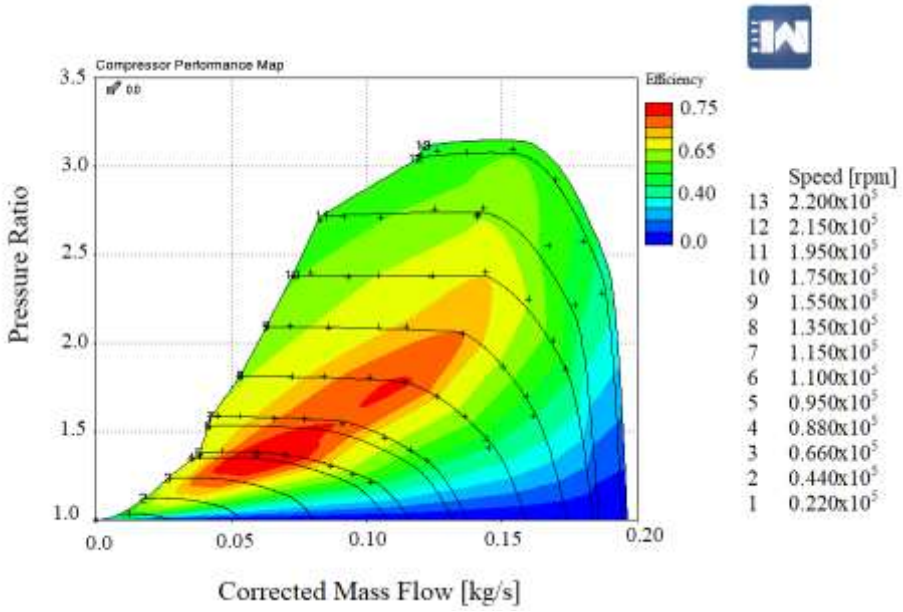

Figure 2. Typical map of a compressor

Even with the scaling laws simplified, matching a turbocharger to an engine is a far more difficult task in itself, as the turbomachinery diameter is not chosen but needs to be obtained to provide the desired performance, and this task needs to be accomplished simultaneously for both compressor and turbine. Bell et al. [15] showed good results for scaling process by first identifying the compressor diameter and the torque required from the turbine to reach the necessary boost, yielding good turbocharger performance results at various engine sizes. However, the author does not show whether or not the results were matched to specific engine performances. Nevertheless, Ricardo WAVE balances the turbocharger shaft speed using a torque balance equation, meaning this method is viable [16].

When scaling for pressure ratios, the results shown have a good correlation between differently sized turbomachinery. However, most methods investigated have not considered scaling the efficiency, which leads to the question, should the efficiency be scaled? Or is it acceptable to assume the change as negligible to the final results? The efficiency can be established as a function of the corrected shaft speed and the pressure ratio as shown in Eq. 3 [15].

$$\eta_{isen} = f\left[N_{corr}, \frac{P_u}{P_d}\right] \quad (3)$$

Based on a previous analysis, if the pressure ratio is not changed during the scaling process, then it should be considered as to how much the function is dependent on the corrected shaft speed. In theory with only a small change to the turbomachinery diameter based on Eq. 2, only a small change to the corrected shaft speed would be calculated, thus dependent on the level of influence this parameter has, it could be assumed that the impact to the efficiency is negligible. Comparing this assumption with Fig. 2, it is clear that a significant change to the corrected shaft speed would be needed to affect the efficiency results. Analysis by Ernst et al. [12] demonstrated that 'for small trim variations (4%) the changes in pressure ratio and efficiency are negligible' and therefore scaling for efficiency should only be considered for large variations in trim (24%).

3. Methodology

The present study involves the analysis of an axial turbine design developed by Pesyridis et al [7, 8]. Preliminary design and optimization of the developed axial turbine is reported in the same literature [7, 8]. Ford Eco Boost 1.6 litre petrol engine with a Garrett turbocharger was chosen for the analysis. The selection procedure following the Garrett manual observed that the GT1548 to be best suited for the Ford Ecoboost engine and was thus opted for further study.

The study incudes

(i) Development of a correlated engine model by scaling the original GT1548 turbocharger test results to match the operating performances of the engine model to Ford Eco-Boost 1.6 litre petrol engine data provided by earlier works

(ii) Obtain baseline steady-state performance results of the engine model with the scaled radial turbine implemented

(iii) Develop a transient model within Ricardo WAVE to compare the turbo-lag between the baseline and the new designs.

(iv) Obtain performance maps to be used to implement in all engine models to provide comparative steady-state results between designs.

(v) Conduct inertia testing to obtain an estimated mass moment of the GT1548 turbocharger, and then scale it to the diameters used to match the turbocharger to the engine.

(vi) Obtain all transient turbocharger data to compare the times to reach maximum shaft speed and manifold pressure against the baseline radial turbine.

3.1 Transient one-dimensional engine modelling

The chosen engine modelling software for this study is Ricardo WAVE. Within WAVE there are two methods for performing a transient simulation. The first is built into WAVE and requires the implementation of a control system, the other requires exporting the model using WAVE RT to combine the model within Simulink. The first method was chosen for the present study as it is far less complex to set up, as well as reduces the need for debugging to one software.

With the transient modelling, it is important that the moment of inertia is calculated correctly, taking into consideration all components of the system. Otherwise, the results could be inaccurate and yield only theoretical results. Mishra and Saad [17], indicated a 68% transient response improvement using an electrically assisted compressor. This was achieved without including a moment of inertia for the electrical motor system by applying the assisted torque directly. Similar to this analysis Gilkes et al. [18] have investigated an air injection assist in a turbocharged 2-litre diesel engine, in which the simulation (WAVE RT) suggested an excess of 15 seconds for the compressor to reach the required manifold pressure. Therefore, care should be taken when analysing the results to ensure they are realistic by comparing to real test data reported in literatures.

Real test data from the Ford Motor Company report indicated that for the 2.3 litre engine, the time to reach the desired shaft speed was approximately 2 seconds at most tested conditions, and for HTT and the DualBoostTM, took no longer than 3 seconds [3, 9]. This range is also concurred by results obtained by Eriksson et al. [19] from an engine model that had been fully validated with engine test data that estimated around 2 seconds to reach desired shaft speeds. Therefore it is highly feasible to achieve realistic results, provided the modelling has been set up correctly.

209

210 4 Ricardo wave engine modelling

211 *4.1 Engine model setup*

212 The engine model used in the present study is the Ricardo WAVE engine model of the Ford
213 eco-boost 1.6 litre petrol engine. A few adjustments were made to the engine model. Firstly, the
214 catalytic duct placed after the turbine was removed, as the modelling was causing excessively high
215 static pressures in the exhaust manifold. Also, the length of the duct entering the turbine was
216 increased to 10 mm from 0 mm.
217 The next step in the setting up the model was to implement appropriate parameters for 'SI
218 Weibe Combustion' sub-model used. For this, values for the location of the 50% mass fraction
219 burned point (CA50) position and burn (combustion) duration (BDUR) from 10% - 90% are required.
220 These values have been obtained from literature and are shown in Fig. 3 adapted from [20]. The
221 turboshaft was also changed from fixed speed to a balanced configuration, as fixed speed would
222 result in the compressor absorbing more power than the turbine was providing, and thus be
223 simulating an electrically assisted turbocharger, resulting in fabricated simulation results. As the
224 inertia at the time was not known, the shaft model was changed to use a dimensionless balance
225 parameter which allows the turboshaft to accelerate/decelerate based upon the power balance
226 between the compressor and the turbine [16]. The corresponding engine performance plots of the
227 actual engine are shown in Fig. 4 and Fig. 5 adapted from [20].
228

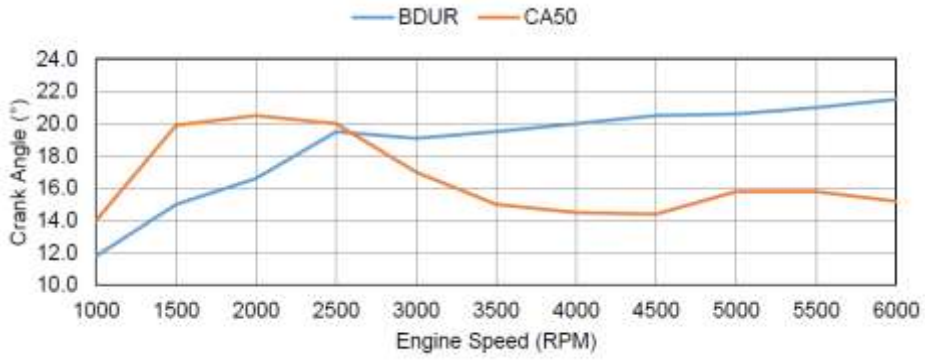

Figure 3. SI Wiebe combustion model parameters [20]

229

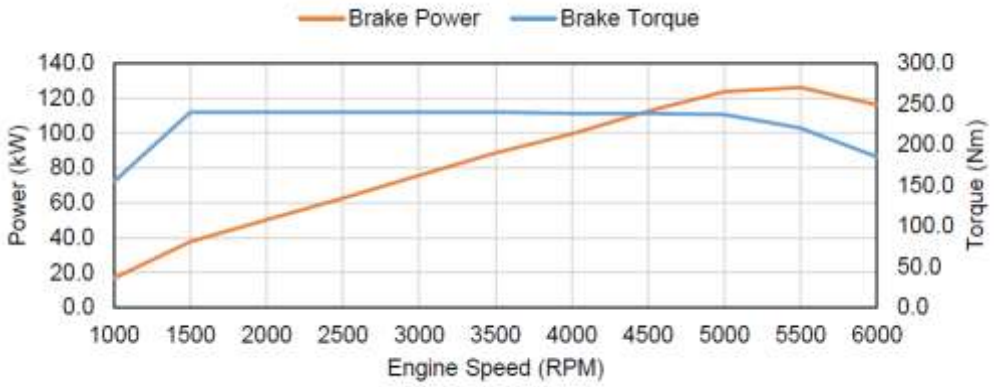

Figure 4. Torque and Power performance of Ford Eco Boost 1.6 litre petrol engine at full load [20]

230

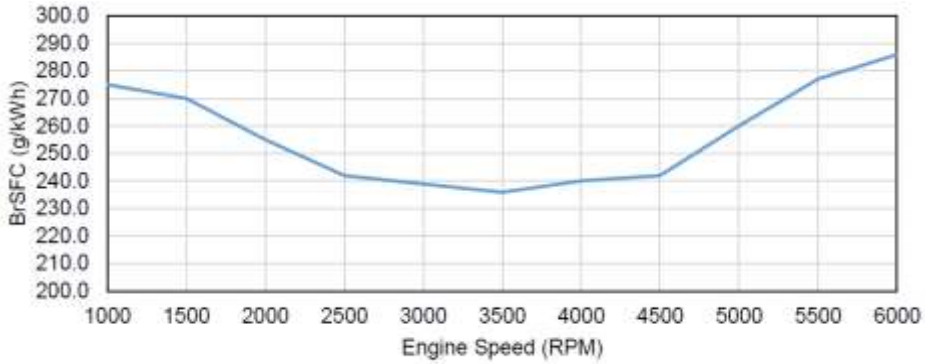

Figure 5. BSFC of Ford Eco Boost 1.6 litre petrol engine at full load [20]

231 *4.2 GT1548 Turbocharger matching to engine*

232 4.2.1 Turbocharger test data implementation

233 The test data from the original GT1548 turbocharger was implemented into the model. The
234 hot-gas test compressor data was used along with the warm-air test data for the turbine. Before
235 implementing the maps into the engine model, the mass flow rates and turbocharger shaft speeds
236 require correction to normalise the raw data to ambient conditions for a direct comparison between
237 the radial and axial turbine results. This is done by using Eq. 4 and Eq. 5. The reference values used
238 are the ones from the test report and are shown in Table 1.
239 The corrected maps are then implemented into the WAVE model, along with the reference
240 conditions and are shown in Fig. 2 and Fig. 6.
241

242 $$m_{corr} = \frac{m\sqrt{T_u/T_{ref}}}{(P_u/P_{ref})} \quad (4)$$

243

244 $$N_{corr} = N_{Tc}/\sqrt{T_u/T_{ref}} \quad (5)$$

245

246 **Table 1**. Reference conditions for conducting turbocharger maps

247

Reference condition	Compressor	Turbine
Pressure	100	101.3
Temperature	298	288

248

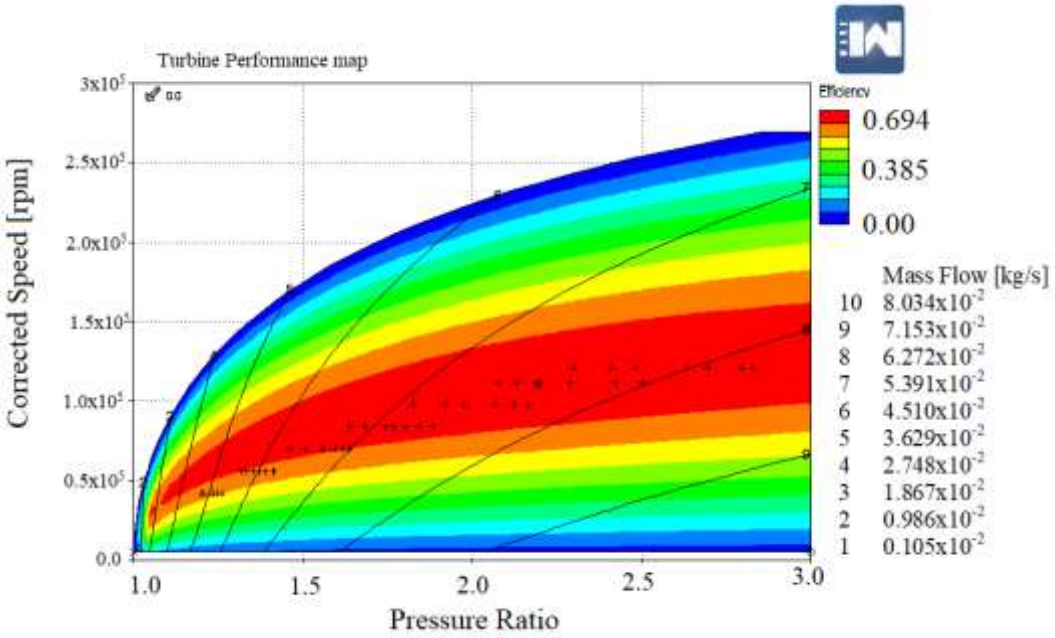

Figure 6. Turbine Ricardo WAVE map

249 4.2.2 Compressor and turbine map scaling

250 The method suggested by Bell et al. [15] was used for scaling the turbocharger maps, as the
251 baseline principles yielded good results for generation of maps with similar performances but at
252 different sizes. Yet the suggested method was not followed in full, as while the method provides
253 conclusive results based on the work conducted, it was unable to provide a methodology that would
254 allow effective engine operating conditions matching. The method was followed until the target
255 parameters were identified, from then on the method utilises an iterative process of a discontinuous
256 function to achieve the compressor outlet and turbine inlet conditions that were tested on the model
257 to provide the correct operating condition at the team's design point.
258 To start the scaling process, both maps are required to be converted into dimensionless maps,
259 representative of the family of compressors and turbines with similar trims [15]. Both maps are
260 scaled using the corrected mass flow rates to obtain the mass flow coefficient (Eq. 6 and 7) and the
261 rotor tip Mach number (Eq. 8 and 9) as a function of the upstream conditions. The results are shown
262 in Fig. 7 and Fig. 8. Note the compressor map was generated using a simple MATLAB script with an
263 interpolation function.
264

$$\phi_C = \frac{\dot{m}_C \sqrt{RT_u}}{P_u D_C^2} \quad (6) \qquad \phi_T = \frac{\dot{m}_T \sqrt{RT_u}}{P_u D_T^2} \quad (7)$$

$$C_{0,C} = \left(\frac{2\pi}{60}\right) N_C \frac{D_C}{\sqrt{\gamma_a R T_u}} \quad (8) \qquad C_{0,T} = \left(\frac{2\pi}{60}\right) N_T \frac{D_T}{\sqrt{\gamma_E R T_u}} \quad (9)$$

265
266

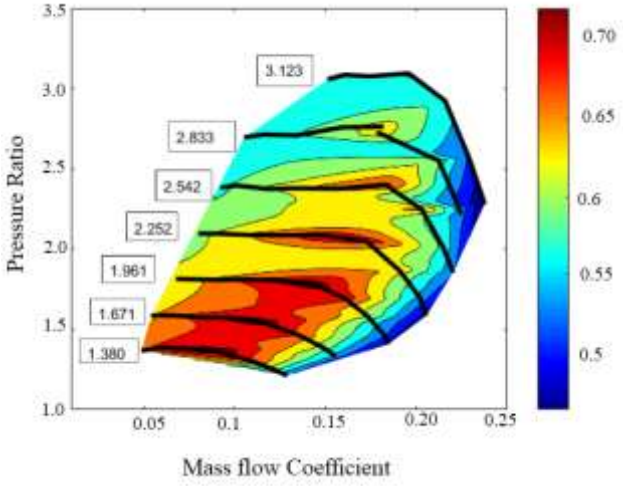

Figure 7. Compressor dimensionless map

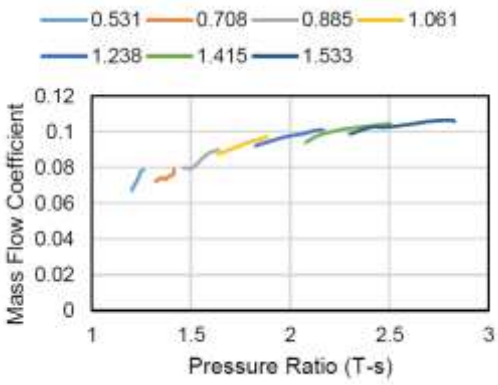

Figure 8. Turbine map for different dimensionless speeds.

With the maps now dimensionless, they can be scaled according to the diameters that match the engine. The next step in the process of scaling the turbocharger maps is to determine the scaled diameters. For this, the air mass flow rate and manifold pressure required to achieve the desired engine performance needs to be calculated [16]. The calculation is done at an engine speed of 5,000 rpm. The mass flow rate was found to be 0.118 kg/s using Eq. 10 and manifold pressure to be 2.14 bar (Eq. 11).

$$\dot{m}_{air} = \frac{\dot{W}\ AFR}{\eta_{TH} E_{LHV}} \tag{10}$$

$$P_m = \frac{120\ \dot{m}_{air}\ RT_m}{\eta_V N_E V_d} \tag{11}$$

The next stage is to determine the inlet conditions of the turbine and outlet conditions of the compressor. This was achieved by following the instructions for calibrating a boosted model set out by WAVE's help manual [21]. The compressor outlet and turbine inlet are disconnected from the model and replaced by ambient ducts. Using WAVE's built-in Design of Experiments tool (DoE), and the Box Benken method of DoE, 25 simulations were conducted varying the compressor outlet conditions and turbine inlet conditions. An empirical equation was then obtained from the results using a multiple regression methodology and a MATLAB script. The script then solved the equation to identify the best combination to achieve the desired engine air mass flow rate. These conditions were then run in the WAVE model to confirm the output matched the predicted empirical response. Finally, the turbine mass flow rate is obtained using the AFR, as while the fuel has combusted, the same amount of mass is expected to flow through the exhaust. The turbine mass flow rate is calculated using Eq. 12. The target parameters are shown in Table 2.

$$\dot{m}_T = \dot{m}_C\ \left(1 + \frac{1}{AFR}\right) \tag{12}$$

Table 2. Target conditions for turbocharger

Parameter	Compressor target	Turbine target
T_{targ}	411 K	1170 K
P_{targ}	2.14 bar	2.65 bar
m_{targ}	0.118 kg/s	0.127 kg/s

With target parameters obtained, the diameters can be calculated using the dimensionless relationship, assuming that the mass flow coefficient is constant for the unscaled and scaled turbocharger maps. Equations 6 and 7 can be equated and re-arranged using the current upstream parameters and the target upstream parameters, resulting in two new equations (Eq. 13 and 14), in which 'ref' subscript denotes the current parameter values and 'targ' denotes the target parameter values [11]. Similarly, Equation 8 and 9 is used to scale the turbocharger speed by taking the average results obtained and is shown in Eq. 15. As the aim of this is to also achieve the correct compressor outlet condition, these were used instead of the inlet conditions to obtain the compressor diameter. The reason this method worked is due to the assumption of the efficiency not changing, and for the target conditions, the power of the compressor absorbed will be the same for the scaled unscaled maps.

$$D_{C,new} = \sqrt{\frac{D_{C,ref}^2 P_{d,targ} \dot{m}_{C,ref} \sqrt{RT_{d,ref}}}{P_{d,ref} \dot{m}_{C,targ} \sqrt{RT_{d,targ}}}} \quad (13)$$

$$D_{T,new} = \sqrt{\frac{D_{T,ref}^2 P_{u,targ} \dot{m}_{T,ref} \sqrt{RT_{u,ref}}}{P_{u,ref} \dot{m}_{T,targ} \sqrt{RT_{u,targ}}}} \quad (14)$$

$$N_{TC} = \frac{1}{2} \left[\frac{N_{T,ref} D_{T,ref} \sqrt{\gamma_E RT_{T,u,targ}}}{D_{T,new} \sqrt{\gamma_E RT_{T,u,ref}}} + \frac{N_{C,ref} D_{C,ref} \sqrt{\gamma_a RT_{C,d,targ}}}{D_{C,new} \sqrt{\gamma_a RT_{C,d,ref}}} \right] \quad (15)$$

Running this calculation once, yielded better performance results, however the maps were still not matched to the engine, and the target conditions were not achieved. It was decided to continue iterating the calculation using Eq. 13, 14 and 15, and updating the reference parameters with the current values.

The final results were then used for the turbocharger maps shown in Fig. 9 and Fig. 10. These maps were then used to identify the correct compressor speeds for the rest of the engine model at full load. It should be noted that comparing the literature it was not necessary to scale the efficiency of the compressor as the scale factor was relatively low (2.1%). However, for the turbine with a scale factor of 29%, it may not have been ideal to assume that the efficiency would not change. Therefore it is possible that the turbine would, in theory, have a higher efficiency and thus a greater power output.

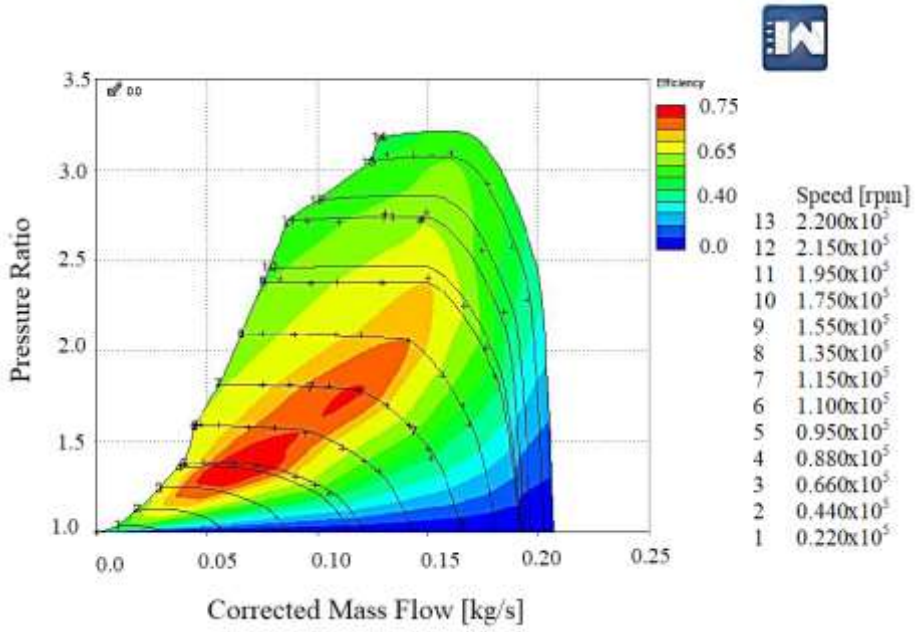

Figure 9. Scaled compressor map

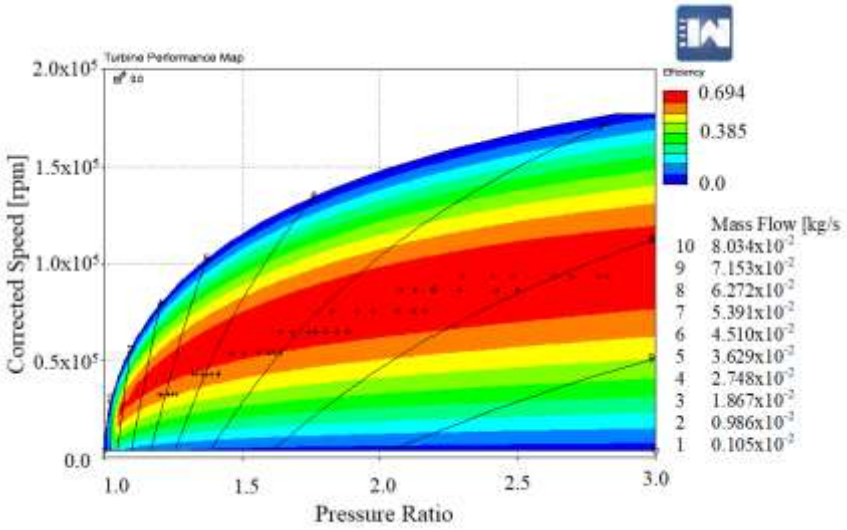

Figure 10. Scaled turbine map

4.2.3 Turbocharger speeds for full load modelling

To identify the correct turbocharger speeds to be used for each full load engine speed, a speed sweep on the turbocharger shaft speed was conducted from 4,000 rpm to 150,000 rpm in intervals of 4,000 rpm. While this speed sweep analysis excessively uses low speeds that would likely not be used for full loading, the data would be used for part load analysis to identify the correct speeds. The reason for this is, during a DoE optimum search procedure run in WAVE, it was identified that the throttle position had minimal impact on the flow rate. The results of the sweep to identify the full load turbocharger shaft speed are shown in Fig. 11 and 12.

The turbocharger speeds were found by interpolating the results for the torque and power that matched the provided data, and then the average speed from both interpolations was used to identify the correct turbocharger speed for each engine speed. The choice of linear interpolation was used as although the profiles of the sweeps are slightly curved when observing the full sweep graphs shown later in Fig. 14, a linear interpolation was used, since it can be reasonably assumed that between relatively small changes in turbocharger speed (4,000 rpm), the response is linear. This assumption is confirmed from Fig. 11 and Fig. 12. For the lower engine speeds (1000 and 2000 rpm) it was noted that the shaft speed would not increase enough to provide the conditions to match the

344 provided data. However, this is to be expected for a few reasons. Firstly, the scaling point of the map
345 (5000 rpm), while chosen to ensure the design point operating conditions were matched to the
346 provided data, may not have been ideal for the lower speeds, resulting in the map performing well
347 at high engine speeds only. The second reason is that the provided data is likely the engine data with
348 the stock turbocharger mounted; therefore it is not easy to match all the operating points of the
349 turbocharger, as the GT1548 is designed to provide more power than the stock turbocharger.
350 Another reason is due to the choice of assuming constant turbine efficiency for the map scaling
351 process. This means the turbine is in theory producing less power as discussed in the previous
352 section, thus resulting in the compressor not receiving enough power to reach higher shaft speeds.
353

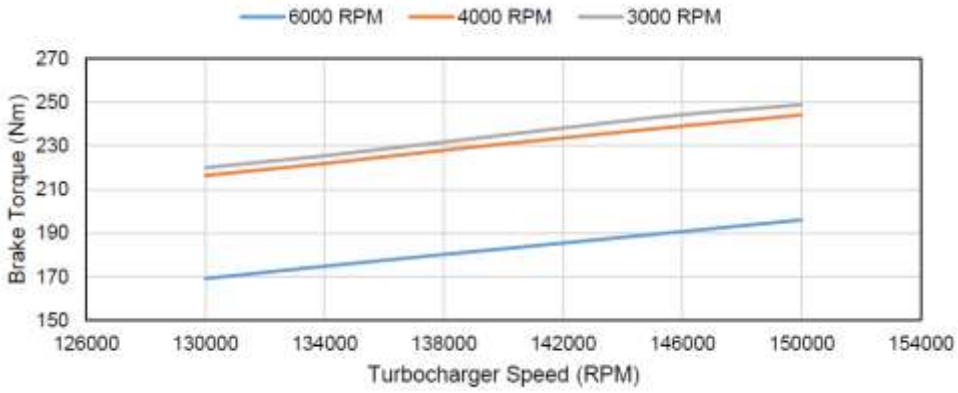

Figure 11. Variation of engine torque during compressor speed sweep at different engine speeds

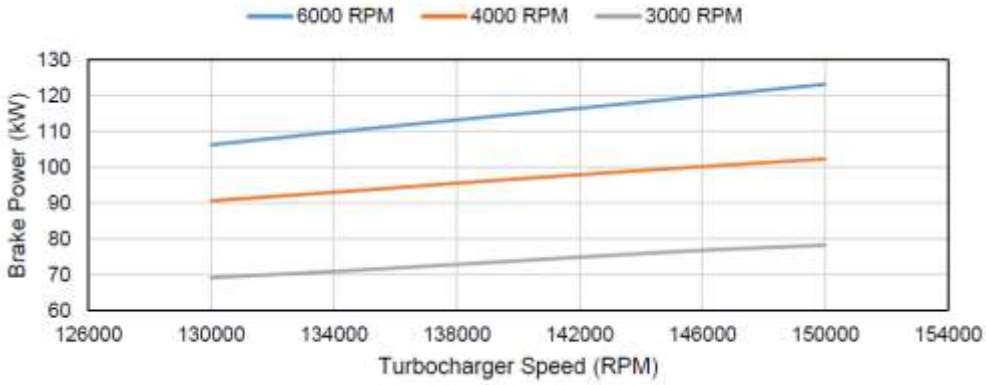

Figure 12. Variation of engine power during compressor speed sweep at different engine speeds

354 4.2.4 Investigation into chosen scaling point effect

355 To confirm the effect of chosen scaling point, the entire scaling process, including the
356 identification of the correct compressor outlet and turbine inlet conditions, was repeated for 3
357 additional engine speeds. The process was conducted for 10 iterations to get an indication of the
358 results, resulting in 30 additional iterations. The diameter results for each engine speed are shown in
359 Table 3. The above results have highlighted two important effects that the chosen scaling point has
360 on the results. Lower engine speeds, where the air mass flow rate is significantly lower results in a
361 larger compressor to increase the pressure sufficiently and the chosen point significantly affects the
362 results. Relative to the compressor, the turbine results, while they have been affected, it is not as
363 significant. Considering the significant variation of the results obtained, it is suggested that, it is a far
364 more sensible and logical option to scale for a mid-range speed, than an end-range speed. Thus
365 ensuring the turbomachinery is better matched at all operating points, and not just at a selected
366 range.

367 Based on this new information, a better clarification on the results for 2000 rpm is understood,
368 and it would have been ideal to use 3000 or 4000 rpm as the chosen scaling point. Nevertheless, the

results thus far have been acceptable for comparable bases as both baseline and new turbines are still going to be tested with the same compressor.

Table 3. Results of scaling for different engine speed performances

Engine Speed	D_C (m)	D_T (m)
1000 rpm	0.05571	0.05186
3000 rpm	0.05253	0.05258
5000 rpm	0.04985	0.05298
6000 rpm	0.04664	0.05308

4.3 Engine modelling validation

The full load results have been compared to the provided engine data and are shown in Fig. 13, 14 and 15. For all but one engine speed, the results correlate well and are within 5% of the data. At 2000 rpm, the results at full load do not correlate with the data provided and is a result of the turbocharger shaft being unable to reach the speed required to deliver the performance data. As discussed previously, the chosen point for map scaling may not have been ideal and the data provided is assumed to be with the stock turbocharger fitted. However, looking at Fig. 16, the BSFC for this speed correlates to within 5% of the provided data and demonstrates that while the target performance is not achieved, the fuel consumption and air mass flow rate results are providing the correct proportion of power. In addition, 3000 rpm is the only point on the graph that is not within 5% (6.03%), indicating a higher consumption than the provided data. This could be a result of the combustion model data that was provided not being correct for the data point, resulting in a higher air mass flow rate needed to achieve the same performance. Nevertheless, the majority of full load conditions are correlated to adequate levels for the purpose of this analysis, and as long as the modelling of the maps are accurate, results can still be compared effectively. It should be noted at this point that 2000 rpm engine speed results should be critically evaluated for realistic values under the transient simulation. The data provided to the team for the chosen design boundary conditions is shown in Table 4.

Figure 13. Comparison between provided engine torque and Ricardo WAVE model

Figure 14. Comparison between provided engine power and Ricardo WAVE model

397

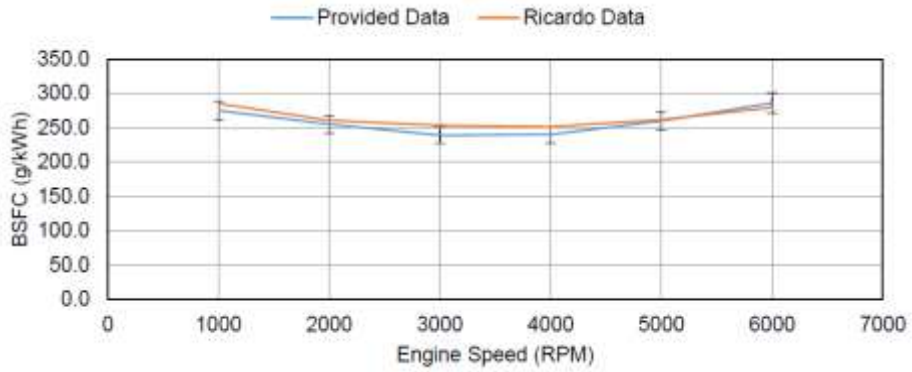

Figure 15. Comparison between provided engine BSFC and Ricardo WAVE model

398

399 **Table 4.** Design point turbine boundary conditions generated in WAVE

Condition	Value
Inlet total pressure (bar)	2.65611
Outlet static pressure (bar)	1.30352
Inlet total temperature (K)	1168.55
Outlet static temperature (K)	1052.44
Mass flow rate (kg/s)	0.1272

400 *4.4 Part load modelling*

401 The part load modelling was achieved by adjusting the turbocharger's shaft speed so that the
402 mass flow rate corresponded to 40%, 60% and 80% of the full load mass flow rate, based on the
403 assumption that engine load is directly proportional to air mass flow rate.
404 To identify the correct turbocharger speed to achieve the appropriate mass flow rate, the
405 previous speed sweep analysis was used from Section 4.2.3. The results for each engine speed are
406 shown below in Fig. 16. To identify which turbocharger speeds should be used for each condition,
407 the results were then linearly interpolated for the mass flow rate that corresponded to the expected
408 part load air mass flow rate for each loading case at each engine speed. The choice of linear
409 interpolation was used, as although the profiles of the sweeps are curved, a linear interpolation was
410 used, since it can be reasonably assumed that between relatively small changes in turbocharger
411 speed (4,000 rpm), the response is linear.
412 The final turbocharger shaft speeds for each loading case are shown below in Table 5 and the
413 mass flow rates for each loading case are shown in Table 6. Using the shaft speeds, the mass flow
414 rates correlated well with the expected mass flow rates and are within 1%. This shows that the choice
415 of linear interpolation was appropriate.
416

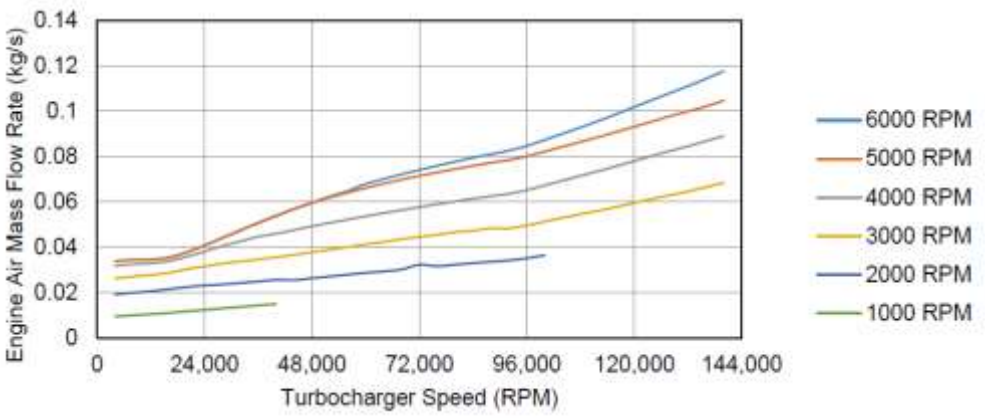

Figure 16. Variation of engine air mass flow rate during compressor speed sweep at each engine speed

Table 5. Turbocharger speed map

N_{TC} (RPM)	Engine speed (RPM)					
Load	**1,000**	**2,000**	**3,000**	**4,000**	**5,000**	**6,000**
100 %	46700	106500	143630	145210	158850	141757
80 %	26978	69536	112308	111906	121476	111412
60 %	5214	24751	63182	64313	69697	66690
40%	n/a	n/a	13395	21609	31429	32202

Table 6. Air mass flow rate at each engine speed and load

m_{ae} (kg/hr)	Engine speed (RPM)					
Load	**1,000**	**2,000**	**3,000**	**4,000**	**5,000**	**6,000**
100 %	57.9623	143.255	257.264	335.677	427.272	433.747
80 %	46.2953	113.751	207.029	269.308	342.331	347.253
60 %	34.8423	85.4361	153.386	202.144	256.701	259.625
40%	n/a	n/a	102.079	132.553	167.475	171.063

5. Results and discussion

5.1 Baseline radial turbine engine data

5.1.1 Baseline performance data

The baseline performance results achieved from the model setup are shown in Fig. 17, 18 and 19. No results were obtained for 40 % part load at low speeds. As previously mentioned modelling of these would require turbocharger shaft speeds of < 0 RPM, which is not possible to model in WAVE and also in real world.

The BSFC results are also as expected, with higher values at lower engine loads due to pumping losses. In addition to this, the validation results (Section 4.3) demonstrated that the BSFC was matched at full load to an acceptable level providing the correct amount of air mass flow rate to the power produced by the engine. Overall the performance results from the model setup, turbocharger matching and part load modelling have resulted in a satisfactory correlation with the engine [22].

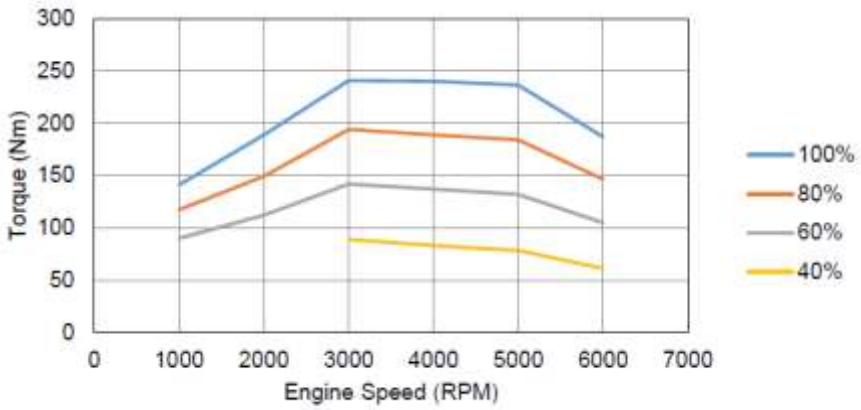

Figure 17. Baseline engine torque at different engine speeds

435

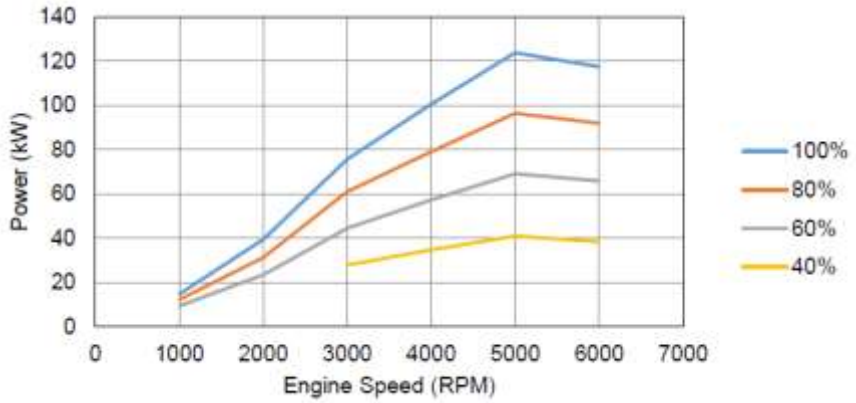

Figure 18. Baseline engine brake power at different engine speeds

436

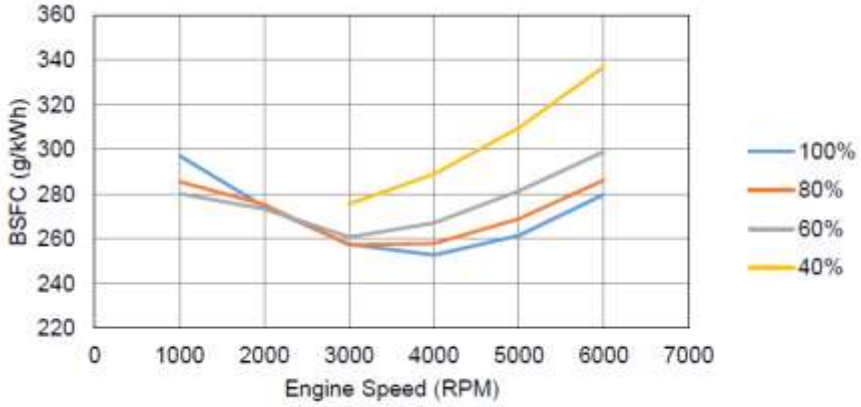

Figure 19. Baseline engine BSFC at different engine speeds

437 5.1.2 Baseline emissions data

438 The baseline emissions results achieved from the model setup are shown in Fig. 20, 21 and 22.
439 The results obtained are only to provide an indication of the effect of the new turbine on the
440 in-cylinder emissions. The NOx results demonstrate higher values at full load in most cases, which is
441 to be expected for the higher air mass flow rate. As more fuel is being burnt to maintain the
442 air-to-fuel ratio, higher will be the combustion cylinder temperatures.

443 Looking at the uHC emissions in Fig. 22, the lower speed emissions at full load do appear to be
444 excessively high relative to the other operating conditions. However, no specific model was used to
445 calculate these emissions and so the default process used in WAVE is likely to over calculate the
446 amount of uHC produced. Nevertheless, this study has only been conducted to provide an

indication of the new turbines effect on emissions and therefore as long as the performance test results show similar correlation, the data is acceptable.

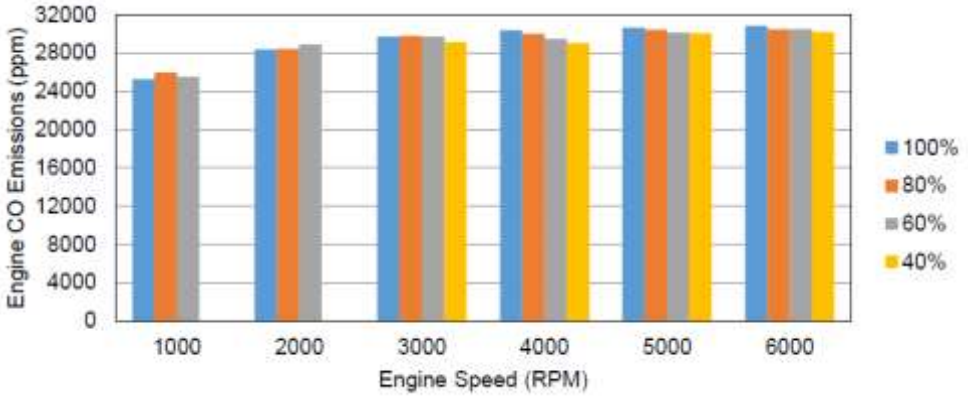

Figure 20. Baseline engine carbon monoxide emissions at different engine loads

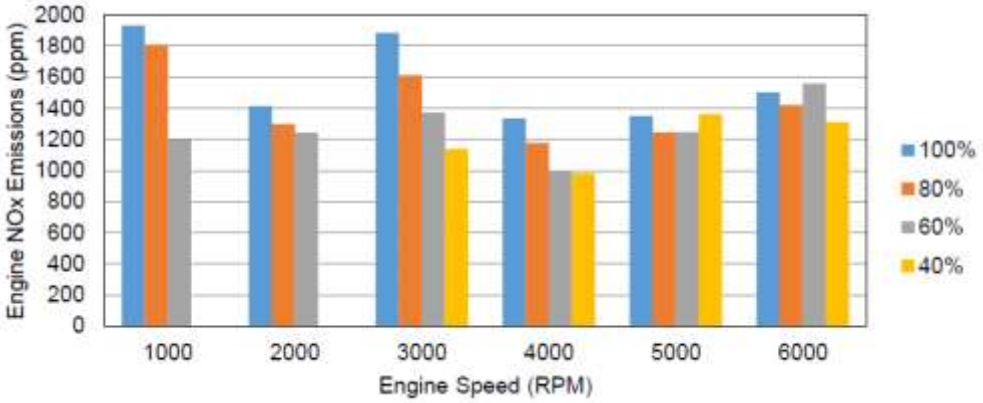

Figure 21. Baseline engine NOx emissions at different engine loads

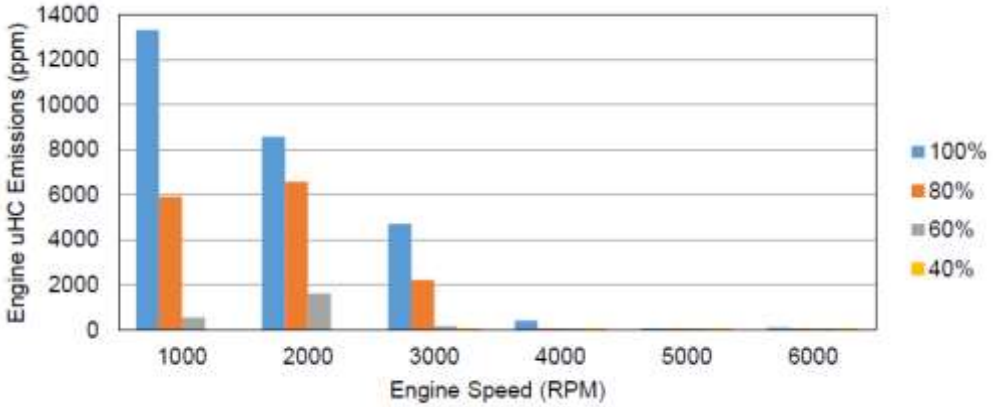

Figure 22. Baseline engine uHC emissions at different engine loads

5.2 Transient Engine modelling

5.2.1 Transient simulation setup

One of the main objectives of this paper is to demonstrate an improved transient response of the turbocharger with the new turbine. As an engine model is already set up and WAVE has the functionality to perform transient calculations, it was chosen to perform the transient analysis. To set

up a transient model, several modifications need to be made to the original model, these were identified by following the setup specified in the user manual [23].

The transient model is created by utilising the steady-state model. The first step in creating a transient model requires the setup of two cases. First, a steady state case is required to initialise the transient simulation. It is necessary to turn off convergence control during the transient modelling as WAVE might stop the simulation part way through, if it deems convergence has been reached. The second case is the initial conditions for the start of the transient simulation. To implement a transient simulation, a composition of an actuator to regulate the engine speed, a control switch and a transient profile are used. The switch is used to change the simulation from the steady-state case to the transient profile and the setup is shown below in Fig. 23. The transient profile is then determined by the user. As the study aims to reduce the time to spool up the turbocharger, a constant engine speed is used from 0-3 seconds as this is the expected maximum duration based on literature [10]. For low load speeds where the exhaust mass flow rate is not sufficient to drive the turbine, the time is increased accordingly.

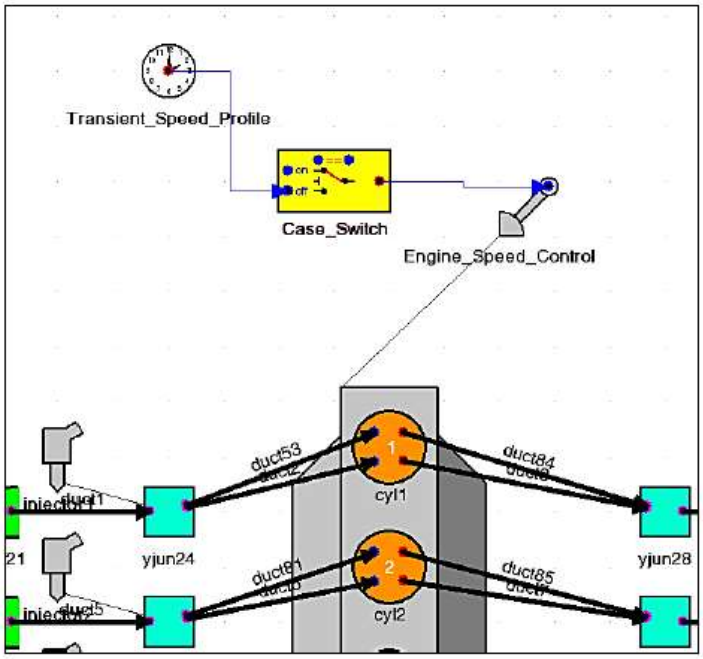

Figure 23. Transient WAVE simulation component setup

Next, the number of cycles for the transient profile needs to be set up properly; otherwise, the simulation may not run for the specified time. WAVE has a pre-generated Excel worksheet to estimate the number of cycles needed to complete the simulation, using a simple integration shown in Eq. 16, where 'ncyc' is the number of cycles required. The user is only required to enter in their specific transient profile, and the sheet can determine the number of cycles required. In WAVE, the number of cycles in the simulation setup is then set as a parameter for each transient case.

$$ncyc = \frac{1}{120}\int_0^{time} N_E\,(t)dt \tag{16}$$

As the engine loading condition does not affect this calculation, the number of cycles for each engine speed is kept constant when simulating part load. The calculated number of cycles required to complete a 3-second transient simulation for a constant engine speed is shown below in Table 7.

Table 7. Number of cycles required to complete a 3 second transient simulation for each engine speed

Engine speed (RPM)	Number of cycles
1000	25
2000	50
3000	75
4000	100
5000	125
6000	150

5.2.2 Inertia testing of GT1548 Turbocharger

With the transient simulation set up, all that is required is the inertia of the turbines. As there is no data available for the GT1548, a simple experiment was conducted to determine the mass moment of inertia of the original turbocharger about its axis of rotation, and then it is scaled up to the matched engine model turbocharger diameters.

The moment of inertia of the turbine was measured by suspending it freely so it could rotate about the shaft axis with string on two sides of the shaft, approximately 180° apart. The shaft is then turned 180°. The turbine was then allowed to oscillate around the axis of rotation until the angular displacement was relatively small. The time to complete 10 and 5 oscillations was then recorded and this was repeated 10 times to get an average time period. This was repeated with the compressor wheel attached. The moment of inertia could then be obtained from Eq. 17, if κ the torsion coefficient of the string used is known [24].

$$I = \kappa \frac{t_p^2}{4\pi^2} \quad (17)$$

If the torsion coefficient is not known, then before being able to obtain the moment of inertia, the string torsion coefficient must be calculated. This is done by repeating the above experiment for a disk of which the inertia is known, and therefore the torsion coefficient of the string can be obtained using the previous equation. In this specific case, the torsion coefficient of the string was calculated to be 0.0002266. With both inertias now obtained, the calculated compressor wheel moment of inertia is given in Table 8.

Table 8. Experimentally obtained mass moment of inertia for GT1548 turbocharger

Turbocharger	Turbine	Compressor
Moment of Inertia (kg/m^2)	Moment of Inertia (kg/m^2)	Moment of Inertia (kg/m^2)
5.54 x 10^{-6}	4.72 x 10^{-6}	8.22 x 10^{-7}

Once the moment of inertia of the turbocharger has been obtained, it requires scaling up to the matched engine condition. As the turbine and compressor have been scaled differently, their inertia needs to be scaled up separately according to the scale factor. The final results are shown in Table 9.

Table 9. Results of inertia testing of GT1548 turbocharger

Parameter	GT 1548 Turbocharger	GT1548 Scaled Turbocharger	Scale factor
Compressor diameter	0.048 m	0.04902 m	1.02125
Turbine diameter	0.0412 m	0.05343 m	1.29684
Compressor inertia	$8.22x10^{-7}$ $kg\ m^2$	$9.13x10^{-7}$ $kg\ m^2$	$(1.02125)^5$
Turbine inertia	$4.72x10^{-6}$ $kg\ m^2$	$1.73x10^{-5}$ $kg\ m^2$	$(1.29684)^5$
Turbocharger inertia	$5.54x10^{-6}$ $kg\ m^2$	$1.82x10^{-5}$ $kg\ m^2$	n/a

This method has obtained a realistic value of the moment of inertia of the original turbine scaled up, which correlates well with the axial turbine of the same diameter. Finally, the inertia has been

implemented into the transient model with the shaft model switch from dimensionless balance parameter to inertia, to provide the actual transient responses.

5.2.3 Baseline transient response

The baseline transient results are shown in Fig. 24. The results are realistic compared with literature experimental and numerical results, with 3 points in excess of 2 seconds and one point well above what was expected [3], [9]. At 2000 rpm full load, the time to reach maximum shaft speed is 5.16 seconds. However, as previously discussed in the model validation (Section 4.3), the performance at this speed was the only exception for the entire model, but the ratio of power to fuel mass flow rate was matched to that of the original engine. Looking at the trend of each speed at their part loading, the results show a consistent percentage change for all engine speeds, with 2000 RPM being the exception.

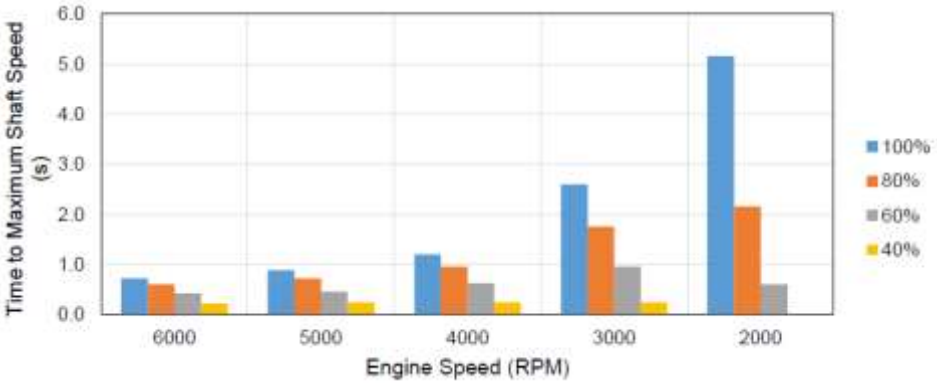

Figure 24. Baseline time to reach maximum shaft speed at various engine speeds and loads

5.3 Turbine map generation

5.3.1 Axial turbine map generation

Generating the map in WAVE requires a minimum of 5 constant speed lines with at least 7 mass flow rates for each speed line. As WAVE's fitting algorithm performs better with more lines, a total of 7 speeds lines were chosen. With the design point being one of the constant speed lines, additional speeds need to be selected. The speeds were chosen to correspond with the current operating conditions of the engine range with enough spacing between each line to achieve a complete profile of the corrected mass flow rate against the total to static pressure ratio. The selected points are shown in Table 10.

Table 10. Turbocharger shaft speed based on engine model operating conditions for map generation

Engine speed (rpm)	Load (%)	Turbocharger speed (rpm)
5000	100	158850
3000	100	143360
5000	80	121476
2000	100	106500
2000	80	69536
1000	100	46700
1000	80	26978

The performance map was generated by utilising ANSYS 'Performance Map' module, in which the design point operating conditions for turbocharger speed and mass flow rate are input, and then

548 several speed lines can be generated based on their percentage of the design point condition. The
549 module can then determine the mass flow rates for each speed line to be run. These are then linked
550 to the optimisation CFX setup that is already created to test the new blade under these conditions.
551 The mesh specification and numerical methodology employed for the CFD analysis are reported in
552 an earlier publication related to this project [7]. Figure 25 and 26 shows the mass flow rates and
553 efficiencies for each map points. It is important to note that the stage efficiencies and pressure ratios
554 have been obtained and not the full system efficiencies and pressure ratios of the final design.
555 However, the data is satisfactory enough to allow the implementation of the Axial Turbine and VGT.
556 With the data obtained, the shaft speeds and mass flow rates are normalised to ambient conditions
557 to allow a comparison with the radial turbine. This is done by following the process outlined in
558 Section 4.2.
559

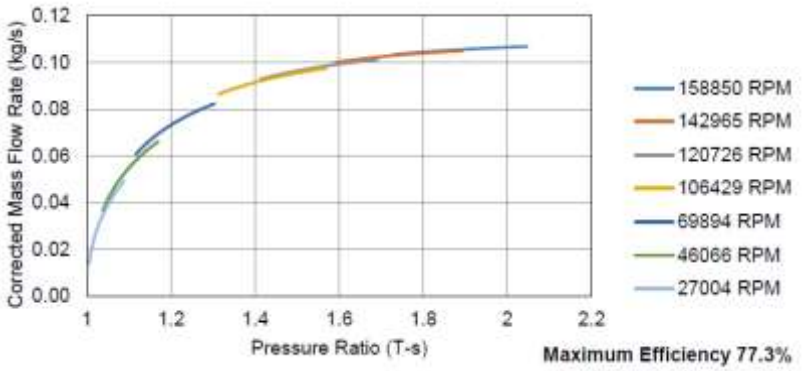

Figure 25. Mass flow rate vs pressure ratio plots at constant shaft speeds for axial turbine

560

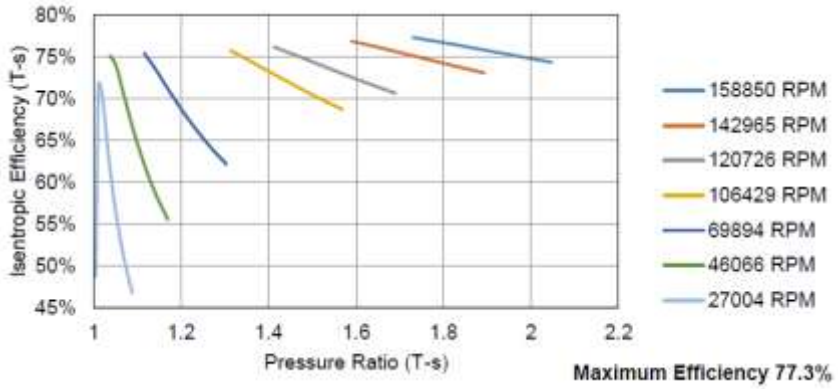

Figure 26. Total to static efficiency vs pressure ratio plots at constant shaft speeds for axial turbine

561

562 Overall the result shows that the majority of the corrected mass flow rate profile was captured
563 and results have allowed for the generation of the maps in WAVE. While the design point yielded an
564 efficiency of 75.87%, the maximum efficiency of the blades is actually achieved at a lower mass flow
565 rate (0.1143 kg/s) along 158850 RPM speed line, and it is 77.3%. Yet, this is to be expected, as the
566 optimisation was set up to find the best compromise between power generation and efficiency. So
567 while this efficiency is higher, it is likely at this test point that the power is lower than at design
568 point.

569 5.3.2 Variable nozzle axial turbine map generation

570 Once the setup of the variable stator pivot angles to be tested had been decided, the map
571 generation was conducted using the same method that was used to generate the original axial
572 turbine map (Section 5.3.1). The same speed lines and mass flow rates were used, but the process had
573 to be repeated for each rack position, this led to a total of 343 CFD simulations to generate all rack
574 positions. Once the results were obtained they are again corrected to normalise them to ambient

conditions (Fig. 27 and Fig. 28). As before, it should be noted that these maps are based on the flow across the blade stage and are not representative of the full system. Overall the result show that the variable geometry setup significantly affects the flow conditions of the turbine, providing higher efficiencies at lower pressure ratios than the original fixed geometry.

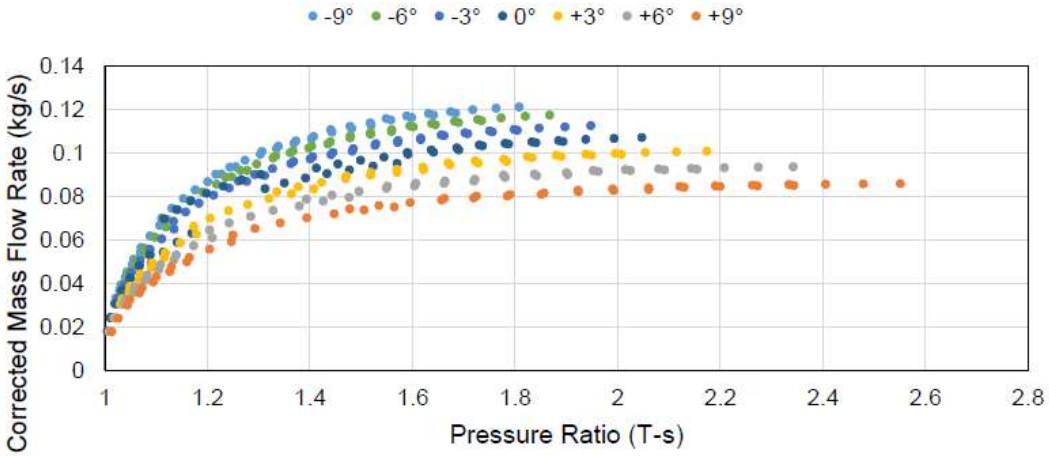

Figure 27. Corrected mass flow rate vs pressure ratio plots at constant shaft speeds at different rack positions for VNT

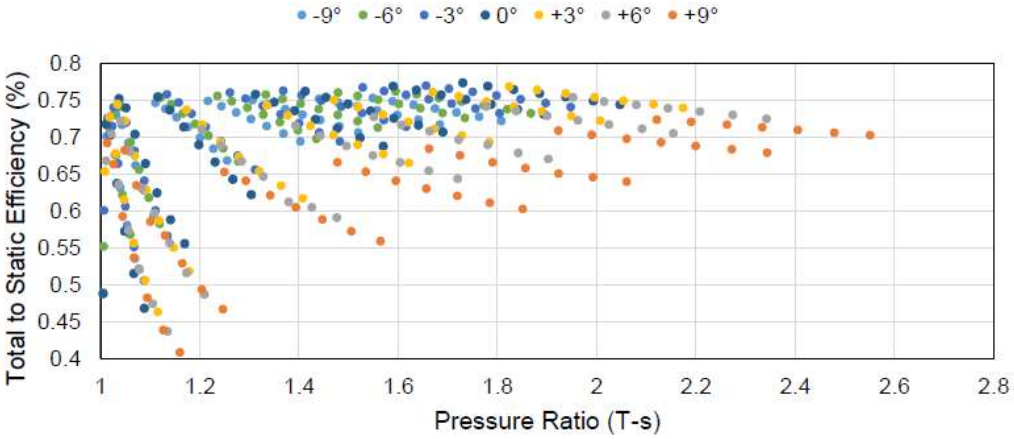

Figure 28. Total to static efficiency vs pressure ratio plots at constant shaft speeds at different rack positions for VNT

5.4 Analysis of Axial Turbine impact on engine performance

5.4.1 Steady state performance comparison

The performance results from the steady-state model between the radial and axial turbine are shown in Fig. 29. Firstly, it can be observed that with the implementation of the axial turbine the engine has better performance at most operating conditions (Fig. 29a and 29b), even though the compressor is still spinning at the same speed. This is likely due to high mass flow rates as a result of lower back pressure to the engine due to better flow expansion of flow by the turbine. However, 2000 rpm at 100% load is the only design point in which the performance is poor than the baseline. This is likely due to the choice of scaling for the design point as discussed in Section 4.2.4.

Observing the BSFC results (Fig. 29c), for most operating conditions the BSFC for axial turbines compared to radial turbines mostly remains same or if not slightly better due to improved performance. This demonstrates the benefit of the axial turbine with regards to fuel consumption, as the engine has not been re- calibrated, and for most cases aside from 2000 rpm at 100% load the power produced is always greater (Fig. 29d). This shows the turbine is capable of producing the

same power as of a radial turbine for a reduced exhaust gas mass flow rate, which in turn allows for increasing the air-to-fuel ratio during re-calibration. Consequently, fuel consumption will decrease, further demonstrating the improvement of the newly designed axial turbine.

Looking at the final graph (Fig. 29 (e)), the axial turbine provides higher efficiencies at all operating conditions of engine. But this is not correspondingly reflected in the turbine power plot in Fig. 29d. For the axial turbines, the figure does not show a significant increase in power, or in some case it actually shows less power (compared to radial turbines) at lower speeds and high loads (Fig. 29d). This could be a result of the difference in map performance, as the axial turbine pressure ratio could be lower at this point, and therefore even though the efficiency is higher, there is not enough power available.

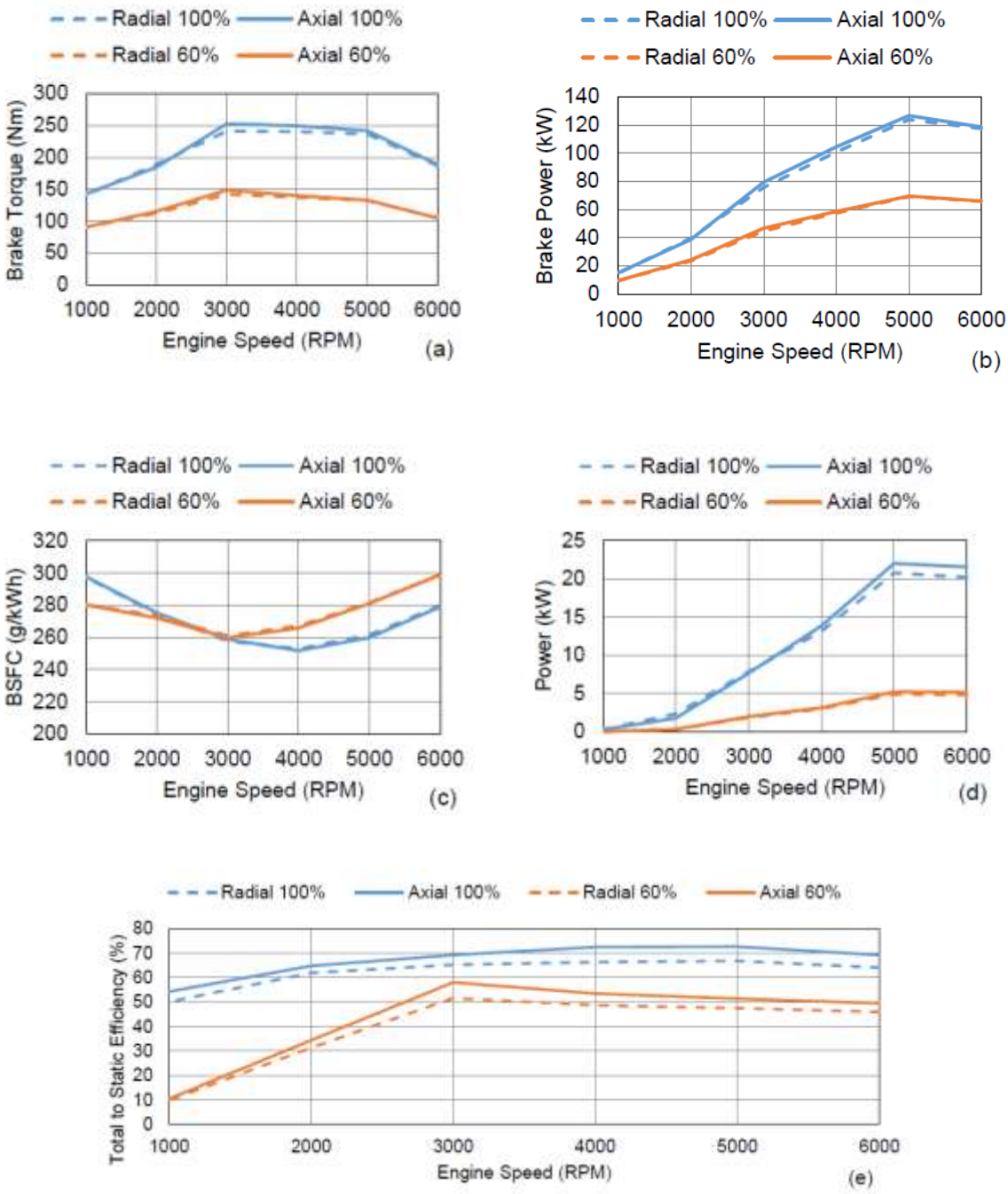

Figure 29. Comparison of (a) Engine brake torque (b) Engine brake power (c) Engine BSFC (d) Turbine power and (e) Turbine efficiency between radial and axial turbine at different engine operating conditions

604 5.4.2 Steady state emissions comparison

605 The results of the comparison between the radial and axial turbine emissions are shown in Fig.
606 30. A common trend noted in the comparison is the axial turbine results show an increase in the
607 in-cylinder emissions at most operating conditions. This demonstrates that by just implementing the
608 new turbine would have a negative impact on emission. This is likely a result of the increased air
609 mass flow rate into the system due to the better expansion of the exhaust flow by the turbine,
610 consequently burning more fuel and producing emissions. However, it should be considered that
611 when implementing a new turbocharger, or new component that affects the way the engine
612 operates, a re-calibration activity should also follow. But this was not attempted in this study.
613 Nevertheless, the new turbine is producing more power than its radial counterpart which means the
614 turbine requires a lower mass flow rate to produce the same power. Therefore, the air to fuel ratio
615 can be increased, reducing the amount of fuel flowing into the engine and thus reducing the
616 in-cylinder emissions.
617

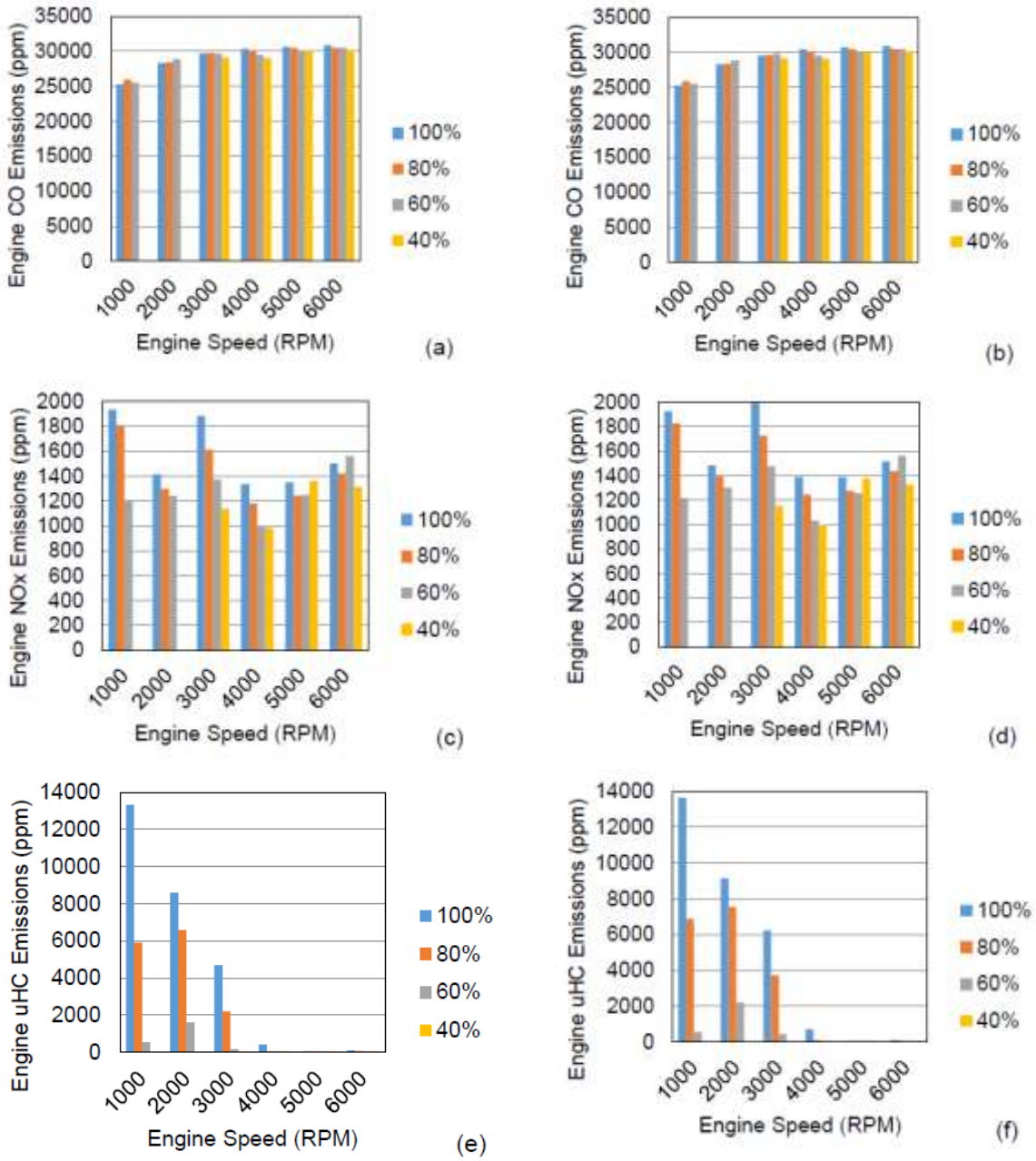

Figure 30. Comparison of engine cylinder emissions between radial (a, c, e) and axial turbines (b, d, f) at different engine operating conditions

618 5.4.3 Transient response comparison

619 A direct comparison between the radial and axial turbine time to maximum shaft speed is
620 shown in Fig. 31. The maximum improvement on transient response was 21.05 % and the minimum
621 was 3.49 % with an average 11.76 % across all engine conditions. The spool up times are in line with
622 the literature with a maximum of 2-3 seconds. However, the improvement does not fully correlate
623 with the results available in the literature. This is expected, as the turbine in this study is designed to
624 be of same size as of the radial turbine. As demonstrated in Fig. 29, the axial turbine produces more
625 power compared to the radial. Therefore if the diameter was reduced, mass reduction could have
626 been achieved, decreasing the mass moment of inertia and likely correlating with the literature
627 results of 25%- 40% improvement. The results however, demonstrate an improved transient
628 response at all operating conditions of the engine. The map and inertia could also be scaled to lower
629 diameter using the methodologies discussed earlier. Using this new data a greater improvement of
630 transient response could be achieved.
631 It should also be noted that the spool up time of 2000 rpm at 100% load does not correlate well
632 with those reported in the literature [3], [9]. This was probably due to the choice of scaling for the
633 design point (Section 4.2.4).

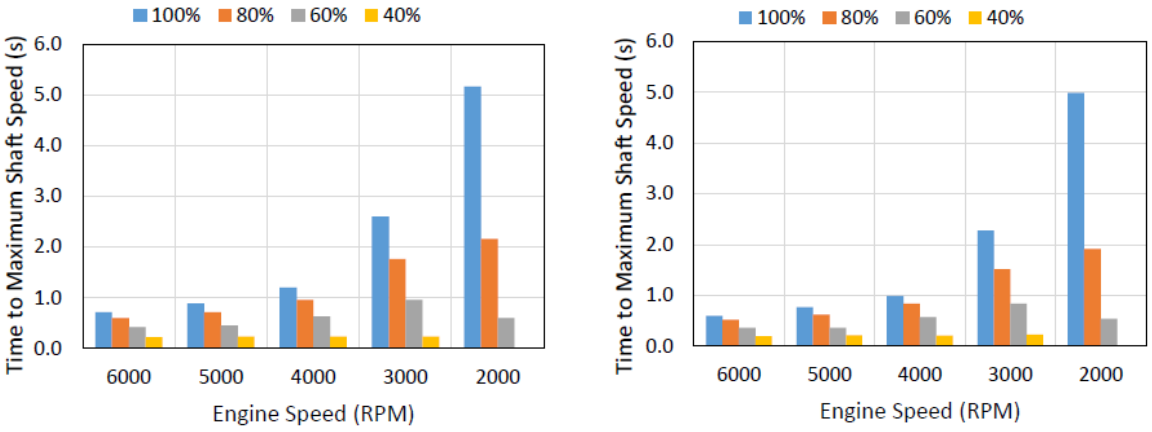

Figure 31. Comparison between radial (left) and axial (right) turbines time to maximum shaft speed at different engine operating conditions

634
635 Figure 32 shows the transient profiles of six different engine conditions, showing the profiles of
636 the shaft speeds and manifold pressures over a 3-second transient simulation. The results are
637 realistic with small improvement at lower loads. This is mainly due to the lower maximum
638 rotational speed needed to be achieved, as well as the likely insufficient exhaust flow fundamentally
639 contributing to the turbo-lag at these operating conditions.
640
641
642
643
644
645
646
647
648
649
650
651

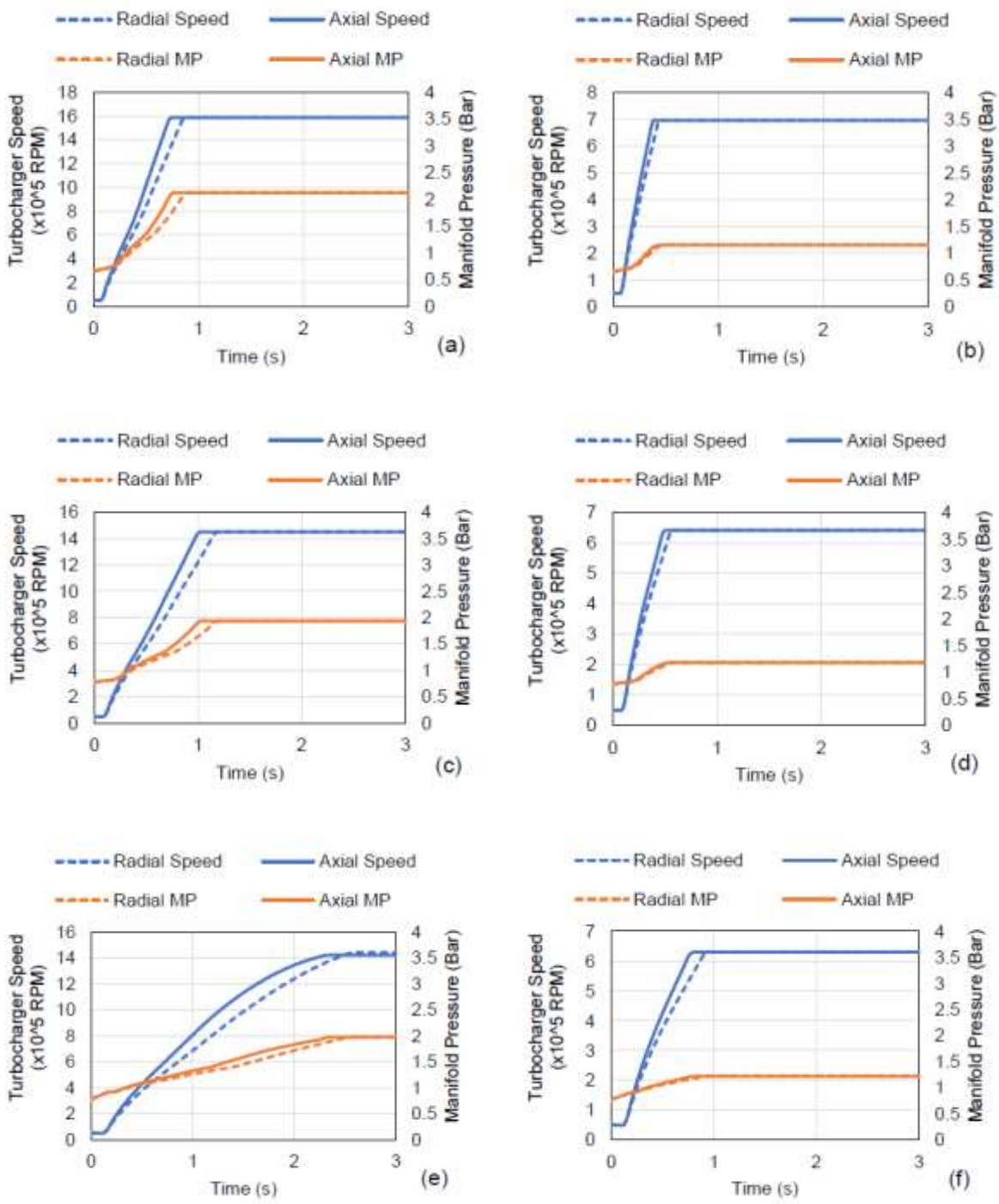

Figure 32. Transient response profiles for turbocharger shaft speed and manifold pressure at engine speeds of 5000 rpm (a, b), 4000 rpm (c, d) and 3000 rpm (e, f) at 100% (left) and 60% (right) engine loads

652

653

654

655

656 5.5 Comparison of moment of Inertia

657 A Genetic Algorithm based optimisation technique was used for the turbine design
658 optimisation [25]. Figure 33a and 33b shows the 3D model of the optimized turbine blade wheel and
659 the turbine respectively. Once the 3D model was generated, finite element analysis was performed
660 to determine the moment of inertia and the factor of safety. The comparison of the moment of inertia
661 and the factor of safety between the radial, initial axial and optimised axial turbine design is shown
662 in Table 11. The table shows that the use of axial turbine has reduced the mass moment of inertia by
663 around 35% without compromising much on the safety factor.
664

Figure 33a. Optimized blade design

Figure 33b. 3D model of the axial turbine

665

666 T**able 11.** Comparison of baseline radial, axial turbine and optimised axial turbine design

	Radial turbine	**Axial turbine (initial design)**	**Axial turbine (optimized design)**
Mass (g)	226.76	112.93	85.41
Mass moment of inertia (kg/m^2)	$1.82x10^{-5}$	$1.59x10^{-5}$	$1.16x10^{-5}$
Safety Factor	NA	2.38	2.16

667 **6. Conclusion**

668 This paper has investigated the preliminary performance difference provided to an established
669 mass production engine, between a radial and axial turbine and by comparison, an improved
670 transient response has been demonstrated. The major conclusions from this study are as follows.
671 The engine model has been successfully validated using real engine test data.
672 It was observed that the effect of choice of design point for scaling has significant impact on the
673 results, especially for the compressor diameter and therefore choice of design point or scaling for
674 multiple design points should be considered.
675 The transient model was successfully developed and provided realistic results for transient
676 response of the turbocharger.
677 A performance map for axial turbine was obtained with a maximum efficiency of 77.3%, the
678 map was implemented into WAVE and comparative results were obtained.
679 The GT1548 turbocharger inertia was successfully calculated from experimental testing and
680 scaled up to the matched diameters to provide an inertia, to the same order of magnitude as the
681 designed axial turbine of similar diameter.
682 The transient response of the axial turbine demonstrated an average of 11.76% improvement
683 with a maximum of 21.05% over its radial counterpart.
684 The performance difference provides further encouragement to further pursue efforts to fully
685 validate the new turbocharger turbine in an engine test bed.

Author Contributions: Gregory Guarda was the research student that conducted the detailed study and wrote the report. Dr Ashish Alex Sam who added expertise and edited the paper. Apostolos Pesyridis is the turbomachinery group leader in the Centre of Advanced Powertrains and Fuels (CAPF) at Brunel University London, who conceived of the project, the layout of the investigations and checked the outcome of the results and subsequent discussion.

Funding: The authors would like to thank the UK's Engineering and Physical Sciences Research Council (EPSRC) for its support through its Impact Acceleration Account programme with internal research code R33339 (11573109).

Conflicts of Interest: The authors declare no conflict of interest.

Nomenclature

AFR	Air to fuel ratio
$c_{o,c}$	Compressor rotor tip Mach number based on inlet conditions
$c_{o,T}$	Turbine rotor tip Mach number based on inlet conditions
D	Diameter (m)
D_C	Diameter of compressor wheel (m)
D_T	Diameter of turbine wheel (m)
E_{LHV}	Lower heating value of the fuel (J/kg)
M_n	Mach number based on inlet flow conditions
$\dot{m}_{air}$	Engine air mass flow rate (kg/s)
$\dot{m}_c$	Compressor mass flow rate (kg/s)
$\dot{m}_{c,corr}$	Compressor corrected mass flow rate (kg/s)
$\dot{m}_T$	Turbine mass flow rate
$\dot{m}_{T,corr}$	Turbine corrected mass flow rate
N_C	Compressor speed (rpm)
N_{corr}	Turbocharger corrected speed (rpm)
N_T	Turbine wheel speed (rpm)
N_E	Engine speed (rpm)
N_{TC}	Turbocharge speed (rpm)
ncyc	Number of cycles required to complete transient engine speed profile
P_d	Pressure downstream (Pa)
P_m	Intake manifold pressure (Pa)
P_u	Pressure upstream (Pa)
R_e	Reynolds number
T_d	Temperature downstream (K)
T_u	Temperature upstream (K)
T_m	Intake manifold temperature (K)
t_p	Time period (s)
I	Moment of inertia
$\dot{W}$	Engine power (W)
V_d	Engine displacement (m^3)
κ	Torsion coefficient
ϕ_C	Non-dimensional mass flow coefficient of compressor
ϕ_T	Non-dimensional mass flow coefficient of turbine
γ_a	Ratio of specific heats of air
γ_e	Ratio of specific heats of exhaust gas
η_{th}	Engine thermal efficiency
η_v	Engine volumetric efficiency

Subscripts

t	Turbine wheel
c	Compressor wheel
ref	current parameter values
targ	target parameter values
new	new parameter values

References

1. Rajoo, S., Romagnoli, A., Martinez-Botas, R., Pesiridis, A., Copeland, C. and Bin Mamat, A.M.I. Automotive exhaust power and waste heat recovery technologies. Book chapter in "Automotive Exhaust Emissions and Energy Recovery", pages 265 – 281, Nova Science Publishers, Hauppage, NY, USA, 2014, ISBN: 978-1-63321-493-4.
2. Gilles, T., 2014. Engine Power and Performance. In: Automotive Engines: Diagnoses, Repair and Rebuilding 7th Edition. Delmar Cengage Learning, pp. 634-655.
3. Rahnke, C., 1985. Axial Flow Automotive Turbocharger, Dearborn, Michigan: Ford Motor Company.
4. Peng, W., 2008. Fundamental of Turbomachinery. New Jersey: John Wiley & Sons.
5. Abidat, M., Chen, H., Baines, N., C., and Firth, M., R., 1992. Design of a highly loaded mixed flow turbine, Proceedings of the Institution of Mechanical Engineers Part A, vol. 206, no. 2, pp. 95–107.
6. Baines, N., C., Lüddecke, B., Filsinger, D., Ehrhard, J., 2012. On Mixed Flow Turbines for Automotive Turbocharger Applications, International Journal of Rotating Machinery, vol. 2012, article id: 589720.
7. Pesyridis, A., Ferrara, A., Tuccillo, R. and Chen, H., 2017. Conceptual design of an axial turbocharger turbine. Proceedings of ASME Turbo Expo 2017: Gas Turbine Technical Conference and Exposition, Charlotte, North Carolina, USA, July 26-30, 2017.
8. Pesyridis, A., Saccomanno, A., Tuccillo, R., Capobianco, A., 2017. Conceptual Design of a Variable Geometry, Axial Flow Turbocharger Turbine, SAE International, 2017-24-0163.
9. Bauer, H., Bali, C., Donkin, G. and Davies, P., 2012. The Next Generation of Gasoline Turbo Technology. Honeywell Transportation Systems
10. Walsh, G., Berchiolli, M., Guarda, G., Pesyridis, A., 2019. Turbocharger Axial Turbines for High Transient Response, Part 1: A Preliminary Design Methodology. Applied Sciences, vol 9(5), 838.
11. Turton, R., 2012. Principles and practice of scaling laws. In: Principles of Turbomachinery.
12. Ernst, B., Kammeyer, J. and Seume, J. R., 2011. Improved Map Scaling Methods For Small Turbocharger Compressors. ASME 2011 Turbo Expo: Turbine Technical Conference and Exposition, Volume 3, pp. 733-744.
13. Dufour, G., Carbonneau, X., Cazalbou, J.-B. and Chassaing, P., 2006. Practical use of similarity and scaling laws for centrifugal compressor design. ASME Turbo Expo 2006: Power for Land, Sea, and Air, Volume 6, pp. 1131-1140.
14. Wentong, M., Yongwen, L. and Ming, S., 2007. New scaling method for compressor maps using average infinitesimal stage. Chinese Journal of Mechanical Engineering, 20(6), pp. 24-28
15. Bell, C., Zimmerle, D., Bradley, T., Olsen, D. and Young, P., 2016. Scalable turbocharger performance maps for dynamic state-based engine models. International Journal of Engine Research, 17(7), pp. 705-712.
16. Ricardo, 2016a. Turbo Shaft. In: WAVE User Manual. Ricardo, p. 17.13.1.
17. Mishra, R. and Saad, S. M., 2017. Simulation based study on improving the transient response quality of turbocharged diesel engines. Journal of Quality in Maintenance Engineering, 23(3), pp. 297-30
18. Gilkes, O. S., Mishra, R., Rao, H. and Fieldhouse, J. D., 2007. Transient response of turbocharged diesel engine for transient operation using air injection assist system. Proceedings of Computing and Engineering Annual Researchers' Conference 2007: CEARC'07. University of Huddersfield, pp. 1-7.
19. Eriksson, L., Lindell, T., Leufven, O. and Thomasson, A., 2012. Scalable component based modeling for optimizing engines with supercharging, E-boost and turbo-compound concepts. SAE International Journal of Engines, 5(2).
20. Capobianco, A., 2016. Design of a Variable Geometry Axial Flow Turbine for Advanced Turbocharger Application, Università Degli Studi Napoli Federico II.
21. Ricardo, 2016b. Boosted Models. In: WAVE User Manual. Ricardo, p. 3.6.4.

741 22. Pesiridis, A., Salim, W. S. I. W. and Martinez-Botas, R. F. Turbocharger matching methodology for
742 improved exhaust gas energy recovery. Proceedings of the 10th International Conference on
743 Turbochargers and Turbocharging (IMechE '12), pp. 203–218, 2012.
744 23. Ricardo, 2016e. Transient Simulation. In: WAVE User Manual. Ricardo, p. 4.2.15.2.
745 24. University of Colorado Boulder, 2004. Lab M4: The Torsional Pendulum and Moment of Inertia. [Online]
746 Available https://nanooptics.colorado.edu/fileadmin/Teaching/phys1140/lab_manuals/LabManualM4.pdf
747 [Accessed 30 March 2018].
748 25. Berchiolli, M.; Guarda, G.; Walsh, G.; Pesyridis, A. Turbocharger Axial Turbines for High Transient
749 Response, Part 2: Genetic Algorithm Development for Axial Turbine Optimisation. Applied Sciences,
750 2019, vol. 9(13), 2679.
751

752